14th International Conference on Structural Safety and Reliability - ICOSSAR'25
1-6 June, 2025 - Los Angeles California, USA
R. Ghanem, E. Johnson, S. Masri and A. Olivier (Eds)

INTEGRATED PERFORMANCE-BASED WIND COLLAPSE ASSESSMENT OF STRUCTURAL AND ENVELOPE SYSTEMS OF ENGINEERED BUILDINGS

JIELING JIANG[1] AND SEYMOUR M.J. SPENCE[2]

[1] University of Michigan
Ann Arbor, Michigan, USA
jennyjjl@umich.edu

[2] University of Michigan
Ann Arbor, Michigan, USA
smjs@umich.edu

Key words: Building envelope; high-rise structure collapse; performance-based wind engineering; probalistic performance; fragility function

Abstract. Advancements in performance-based wind engineering have significantly enhanced the assessment of engineered building systems. However, the performance of building envelope systems—essential for ensuring life safety—remains insufficiently understood during extreme wind scenarios that can induce strong nonlinear structural behavior, potentially leading to building collapse. This study conducts a comprehensive performance assessment of a high-rise archetype building envelope system while explicitly accounting for the progressively increasing nonlinear structural behavior as structural collapse approaches. The relative severity of damage to the structural and envelope system are discussed as is the general validity of the framework. Key insights are obtained in terms of the evolution and spatial pattern of envelope damage, highlighting the time-dependent and coupled mechanisms that govern the progression of envelope damage. Furthermore, the influence of the choice parameters defining the fragility functions of the envelope system is quantitatively assessed, providing a comprehensive understanding of their effects on the reliability of the envelope system.

1 INTRODUCTION

Over the past few decades, the development of performance-based wind engineering (PBWE) has significantly advanced the performance assessment of engineered building systems [1, 2, 3, 4, 5, 6, 7]. While the structural system has been the primary focus of performance-based assessments, the envelope system has gained increased attention given its vulnerability during extreme wind events. Evidence from past extreme wind events has consistently shown that envelope systems are particularly vulnerable, often sustaining substantial damage that poses critical life safety risks and contributes to major economic losses [8, 9, 10]. These losses are further amplified by secondary hazards such as water ingress [11, 12]. Therefore, a detailed understanding of envelope system performance under extreme wind scenarios is imperative.

Although various contributions have been made in this domain [12, 13, 14], the performance of envelope systems in the context of highly nonlinear structural responses under extreme wind events, up to and including structural collapse, remains insufficiently understood. In particular, the dynamic interaction between the strong nonlinear structural response and the envelope damage, as well as the relative severity of their respective performance states, needs more investigation.

To address this gap, this study integrates a framework for holistic performance assessment of extreme wind-excited coupled structural-envelope systems. Specifically, the envelope performance is investigated in a high-fidelity nonlinear structural modeling environment subjected to collapse-level wind loads. A full-scale, 45-story reinforced concrete archetype building serves as a representative example to examine the coupled behaviour of the structure and its envelope under extreme wind conditions. The study provides a comprehensive assessment of the collapse-level performance of this integrated system.

2 DAMAGE ESTIMATION METHODS

2.1 Nonlinear structural dynamic analysis

For structures experiencing nonlinear behavior under extreme wind loads, estimation of the inelastic dynamic response can be achieved by solving the equations of motion as follows:

$$\mathbf{M}(\mathbf{x}_m)\ddot{\mathbf{u}}(t) + \mathbf{F}_D(\mathbf{u}(t), \dot{\mathbf{u}}(t), \mathbf{x}_m) + \mathbf{F}_R(\mathbf{u}(t), \mathbf{x}_m) = \mathbf{F}(t; v_H, \alpha) \tag{1}$$

where, $\mathbf{M}$ is the mass matrix; $\mathbf{x}_m$ is a vector collecting the random variables associated with the uncertainties in the structural model (e.g., structural material properties and geometric uncertainties); $\ddot{\mathbf{u}}$, $\dot{\mathbf{u}}$ and $\mathbf{u}$ are the vectors of displacement, velocity, and acceleration responses of the structure, respectively; $\mathbf{F}_D$ and $\mathbf{F}_R$ are the nonlinear damping and restoring force vectors that depend on the structural response and structural model uncertainties; $\mathbf{F}(t; v_H, \alpha)$ denotes the stochastic wind load time history for a wind speed of v_H and wind direction of α, obtained by integrating the external wind pressure over the floor tributary areas. To solve Eq. (1) for the strong nonlinear problems and potential structural collapse considered in this work, explicit integration methods can be adopted. Furthermore, to accurately capture structural collapse and enable the propagation of the uncertainties $\mathbf{x}_m$ within the structural system, a high-fidelity nonlinear modeling environment is required.

2.2 Building envelope damage measures

Envelope damage during wind events is inherently progressive and time-dependent, with different damage mechanisms potentially interacting due to the cumulative nature of the damage progression. This study follows the framework proposed by Ouyang and Spence [11, 14], wherein each envelope component is considered to be susceptible to drift-induced and pressure-induced damage. The progressive nature of the damage is captured through a series of N_d sequential drift-induced sequential damage thresholds, denoted as $R_{E_{d,1}} \leq R_{E_{d,2}} \leq ... \leq R_{E_{d,N_d}}$, and N_p sequential pressure-induced damage thresholds, denoted as $R_{E_{p,1}} \leq R_{E_{p,2}} \leq ... \leq R_{E_{p,N_p}}$. The occurrence of a particular damage state implies that all less severe damage states have occurred. At any given time during the wind event, the current damage state of an envelope component is identified as the most severe threshold exceeded up to that point. To preserve the time-dependent progression of damage, the envelope damage state is evaluated and updated at each simulation time step whenever a threshold is crossed. The interaction between drift- and pressure-induced damage is explicitly modeled through degradation of the corresponding resistance: specifically, the occurrence of a drift-induced damage state in

one envelope component will result in a reduction of its capacity to resist the wind pressure, thereby introducing coupling between the two damage mechanisms.

2.3 Collapse failure probability estimation

In this study, the small probability of the occurrence of structural collapse is estimated using a sector-by-sector framework integrated with an optimal stratified sampling scheme, as outlined in [15]. The wind direction is first discretized into equally sized, mutually exclusive sectors. The sector yielding the most critical structural response, referred to as the critical sector, is identified through a preliminary elastic dynamic response analysis. Within the critical sector, the wind hazard curve is described by the exceedance probability of maximum mean hourly wind speed. This curve is further stratified into N_e mutually exclusive and collectively exhaustive strata, each representing a range of wind speeds. Within each stratum S_k, the conditional failure probability $P_{f|S_k}$ corresponding to a given limit state of interest is estimated using standard Monte Carlo simulation. The overall failure probability $\tilde{P}_f$ is then computed using the law of total probability:

$$\tilde{P}_f = \sum_{k=1}^{N_e} P_{f|S_k} P_{S_k} \tag{2}$$

where P_{S_k} denotes the probability that the wind speed falls within stratum S_k, which can be directly obtained from the hazard curve. A key aspect of this methodology is the efficient allocation of samples across strata to ensure accurate estimation of failure probabilities. The optimal sample allocation is determined by solving an optimization problem that minimizes the total number of samples while satisfying a target coefficient of variation (COV) for the estimated failure probability across all strata and limit states of interest [15].

3 ARCHETYPE BUILDING PERFORMANCE ASSESSMENT

3.1 Building and hazard description

A 45-story rectangular reinforced concrete archetype building, with dimension of 45.72m$\times$30.48m $\times$180m, located in New York City, is analyzed following the framework outlined in Sec. 2. The archetype is designed as a risk category II building, targeting a reliability index of 4.0 for widespread progression of damage over a 50-year reference period, corresponding to an annual failure probability of 7.0×10^{-7} as prescribed in ASCE 7-22 [16]. The structural system mainly consists of a centrally located concrete shear wall core and coupling beams, as shown in Fig. 1. Gravity loading is applied through a floor area load of $6.28kN/m^2$ uniformly distributed over each slab, and an envelope cladding weight of $1.2kN/m^2$ distributed over the vertical perimeter surface. The lateral load-resisting capacity is assumed to be provided entirely by the central core. A high-fidelity finite element model is developed in OpenSees [17]. Shear walls are molded using three-dimensional, flexurally dominated four-node shell elements. The coupling beams are modeled through displacement-based beam-column elements. The rigid diagram is applied at each floor. Material nonlinearities in both concrete and reinforcing steel are captured using hysteretic stress-strain models that account for stiffness degradation and strain hardening effects. Uncertainties in material properties and geometric dimensions are characterized using predefined probabilistic distributions, with additional details provided in [18].

The envelope system consists of a total number of 4500 dual-pane laminated insulating glass panels with a size of 1.524 m $\times$ 2 m with a thickness of 6 mm. The building is assumed to be nominally

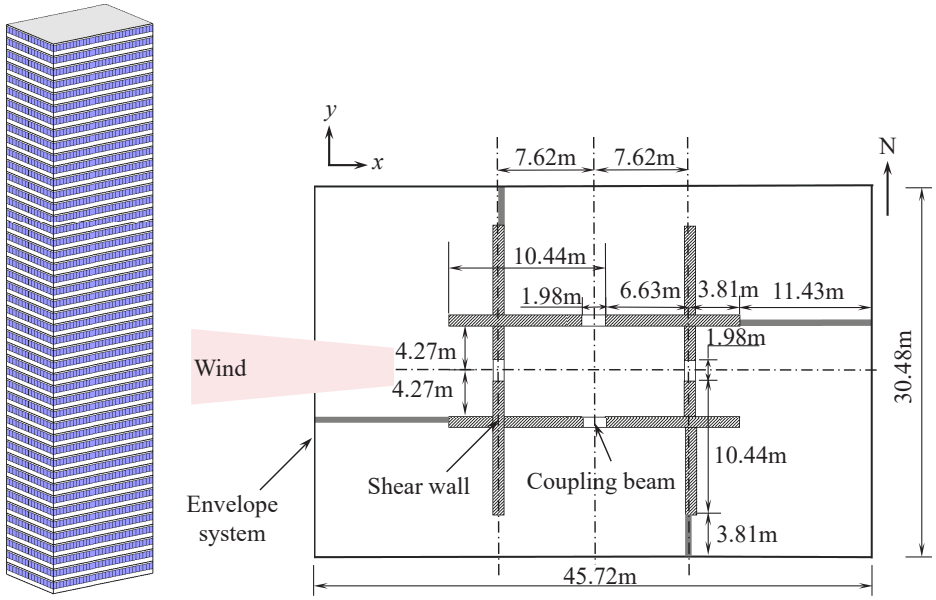

Figure 1: Schematic of the archetype building: (a) 3D view; (b) plan view.

sealed, with no pre-existing damage to the envelope system. Internal pressure within each enclosed interior space is considered spatially uniform. Each envelope component is modeled as being vulnerable to two sequential drift-induced damage states DS_1^d and DS_2^d and one pressure-induced damage state DS^p, with fragility parameters summarized in Table 1. The coupling effect between drift- and pressure-induced damage is incorporated via resistance reduction factors. Specifically, the occurrence of DS_1^d or DS_2^d results in reductions to pressure resistance characterized by truncated normal distributions with means of 0.9 and 0.2, respectively, bounded between [0, 1] and with a standard deviation of 0.1.

Table 1: Fragility functions for the drift- and pressure-induced damage states

Damage state	Mean	Dispersion	Distribution
DS_1^d	0.021 (rad)	0.6	Lognormal [19]
DS_2^d	0.024 (rad)	0.6	Lognormal [19]
DS^p	4.45 (kPa)	0.15	Normal [20]

The non-directional wind hazard curve of the archetype is defined by the Type I distribution, calibrated based on the reference wind speeds derived from the annual 3-s gust wind speeds corresponding to various mean recurrence intervals as specified in the hazard map of ACSE 7-22 [16]. Eight wind sectors are considered to account for the wind directionality effects. The critical sector is determined by the preliminary elastic analysis of the resultant base moment, with the maximum response occurring within the directional range of 247.5° to 292.5°. Accordingly, all subsequent simulations are performed exclusively for this critical wind sector.

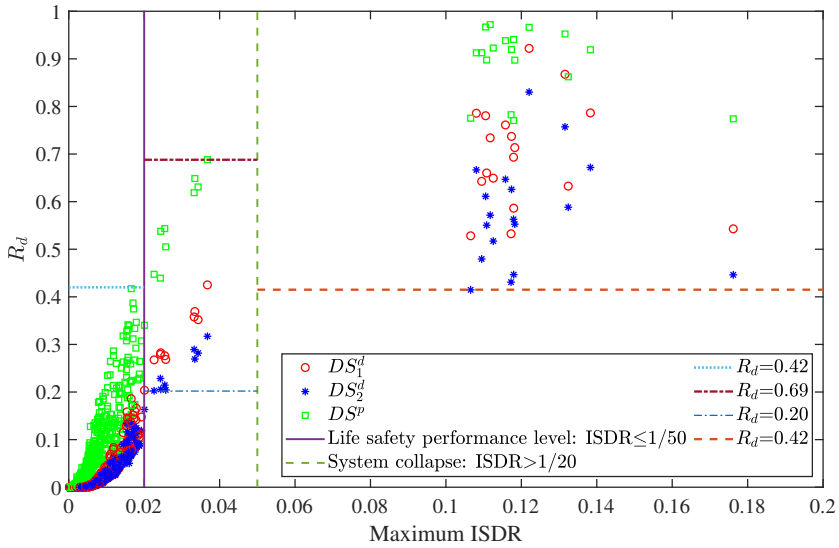

Figure 2: Maximum ISDR vs envelope damage ratio R_d under each simulation.

3.2 Results

3.2.1 Damage severity comparsion

In this study, structural system collapse is defined as the condition in which the maximum inter-story drift ratio (ISDR) exceeds 1/20. To estimate the probability of collapse, a total of 1,011 optimal samples are generated using the optimal stratified sampling approach described in Sec. 2.3 (with target COV of 20%). Each sample represents a realization of the random vector encompassing the model uncertainties, including variability in material properties, geometric dimensions, and wind loading parameters. The resulting probability of failure associated with structural collapse is estimated to approximately 3.5×10^{-6}, with a corresponding coefficient of variation (COV) a little over 20%. This estimate satisfies the target reliability index of 4.0 as prescribed in ASCE 7-22 [16] and shows that the adopted optimal sample allocation is effective in quantifying collapse probability with reasonable accuracy.

To evaluate the relative severity of damage between the structural and envelope systems, Fig. 2 shows the maximum inter-story drift ratio (ISDR) of the structural system along with the envelope damage ratio R_d under damage states DS_1^d, DS_2^d, and DS_p. Two vertical lines are shown to denote the life safety performance threshold and the structural collapse limit state, respectively. Within the life safety performance range, the progression of DS_1^d, DS_2^d, and DS^p exhibits an approximately linear relationship with increasing structural response. At this stage, the maximum R_d can reach up to 42%, even in the absence of structural collapse. DS^p dominates the envelope damage, while the drift-induced damage ratio remains around 20%. As the structural system enters a highly nonlinear regime but remains below the collapse threshold, the maximum envelope damage ratio increases to approximately 69%, with DS^p continuing to be the dominant contributor. The relationship between damage ratios under all three damage states and the maximum ISDR remains approximately linear during this phase. Upon reaching structural collapse, R_d under DS_1^d and DS_2^d increases substantially, nearly doubling, as a result of the large deformation happening in the structural system. At this stage, the maximum R_d under DS_1^d and DS_2^d reaches a limit of 92%, while the maximum R_d under DS^p approaches 98%. This indicates that under collapse-level winds, both the structural and envelope

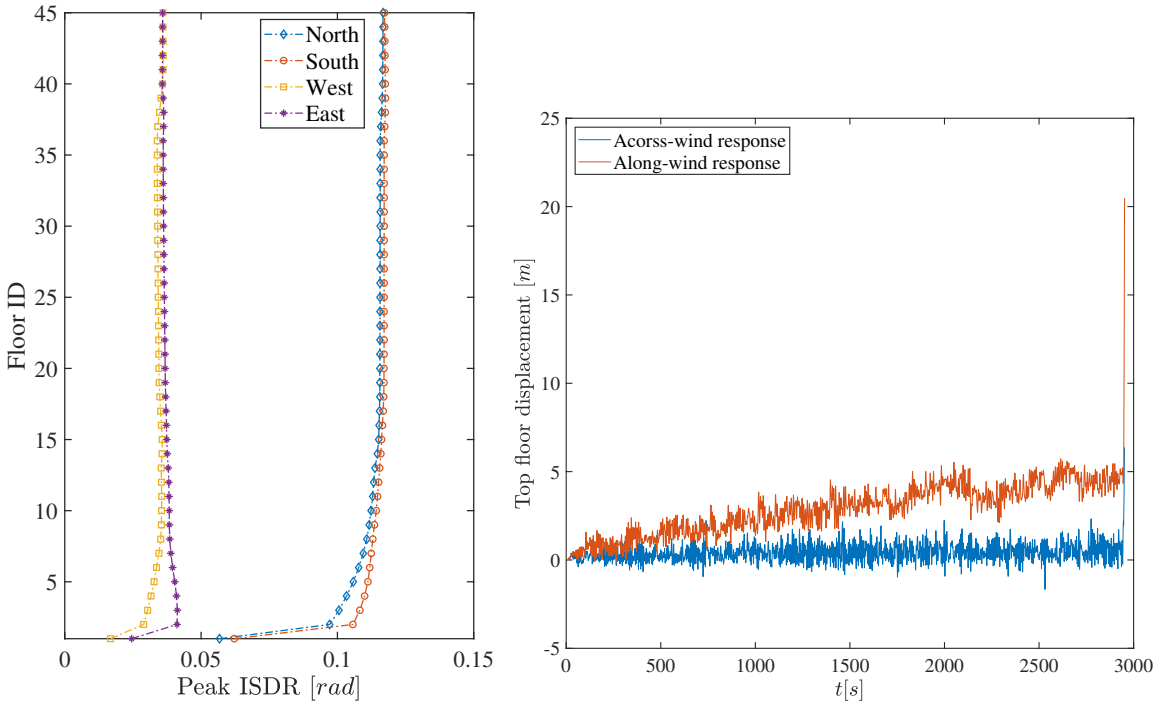

(a) (b)

Figure 3: Structural responses: (a) peak ISDR at four faces of the structure; (b) top floor displacement time history.

systems experience severe damage, leading to a complete loss of functionality.

3.2.2 Damage coupling effects

In this section, one collapse sample is examined in detail. This sample has a wind speed of 95.43 m/s under a wind direction of 250°, resulting in an envelope damage ratio R_d of over 95% under DS^p. Fig. 3 presents the peak ISDR over all floors and the time history of the top floor displacement. It can be observed that the collapse behavior is characterized by simultaneous excessive along-wind and across-wind deformations localized at the first story of the structure.

To further investigate the evolution and coupling behavior across different damage states, Fig. 4 presents the time history of the maximum ISDR at the four faces of the structure. Two vertical lines indicate the moments when the ISDR reaches the life safety performance limit and the impending structural collapse, respectively. Fig. 5 show the corresponding envelope damage maps when the life safety limit state for the structural system is exceeded (i.e., at $t = 986$s), where each block with different colors representing different types of coupling. It can be seen that the envelope components on the north and south faces exhibit increased drift-induced damage, consistent with the higher ISDRs observed on those faces in Fig. 3. Most envelopes that initially experienced DS_1^d transition into DS_2^d due to progressive deformation. At this stage, DS^p is predominantly observed on the west (windward) face, driven primarily by direct wind pressure without coupling effects with the drift-induced damage state. In contrast, the east, north, and south envelopes display damage that is primarily attributed to the coupling between DS^p and the drift-induced damage states, particularly DS_2^d.

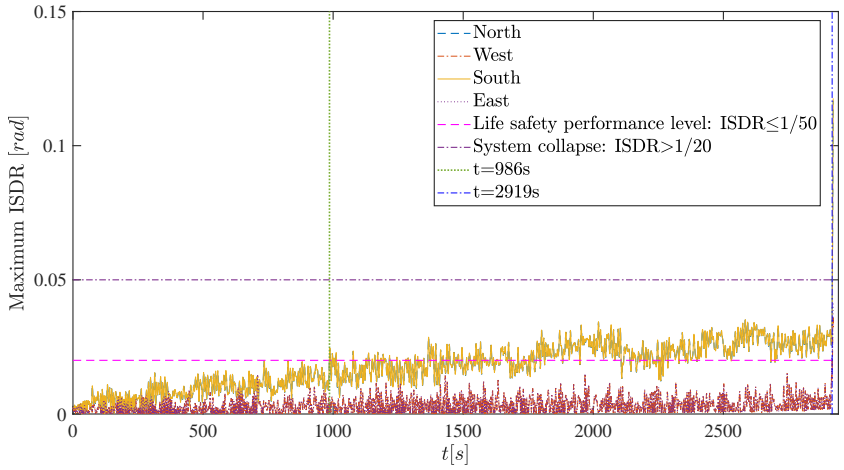

Figure 4: Time history of the maximum ISDR at four faces of the structure.

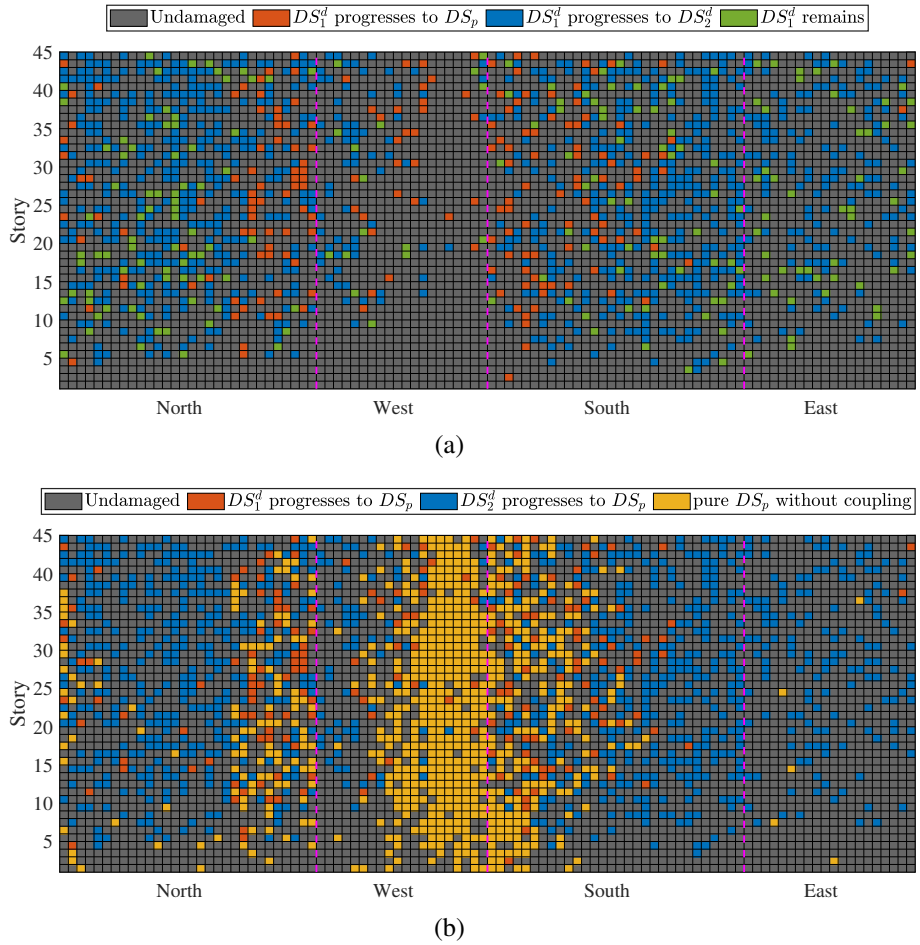

Figure 5: Damage coupling map of the envelope system at $t = 986$s: (a) DS_1^d; (b) DS^p.

4 CONCLUSIONS

This study presents a comprehensive assessment of the coupled behavior between structural and envelope systems in high-rise buildings subjected to collapse-level extreme wind loading. By integrating a high-fidelity nonlinear structural model with a multi-stage, time-dependent envelope damage framework, the analysis effectively captures the dynamic interdependencies between the nonlinear structural response and the envelope damage progression.

A full-scale archetype building located in New York City is analyzed. The estimated collapse probability satisfies the target reliability with a reasonable coefficient of variation, demonstrating the effectiveness of the adopted simulation strategy. A comparative analysis of structural and envelope performance showed the relative severity of damage between the two systems. Specifically, the envelope damage ratio reaches around 40% prior to the structural system exceeding its life safety performance threshold, increases to approximately 70% under highly nonlinear but non-collpase structural conditions, and ultimately increases up to 98% at impending structural collapse. Detailed examination of a collapse sample reveals that the envelope components in the crosswind direction are more susceptible to drift-induced damage, while pressure-induced damage dominates the windward face of the envelope components. Coupling effects between drift and pressure damage states become more pronounced as structural nonlinearity increases, leading to substantial amplification of envelope damage near collapse. These observations highlight the importance of explicitly modeling the interaction between structural and envelope systems in extreme wind scenarios.

5 ACKNOWLEDGEMENTS

This research effort was supported by National Science Foundation (NSF) through grant CMMI-2118488.

REFERENCES

[1] Ciampoli, M., Petrini, F., and Augusti, G. Performance-based wind engineering: towards a general procedure. *Structural Safety*, **33**(6), 367–378, (2011).

[2] Barbato, M., Petrini, F., Unnikrishnan, V. U., and Ciampoli, M. Performance-based hurricane engineering (PBHE) framework. *Structural Safety*, **45**, 24–35, (2013).

[3] Spence, S. M. J., and Kareem, A. Performance-based design and optimization of uncertain wind-excited dynamic building systems. *Engineering Structures*, **78**, 133-144, (2014).

[4] Spence, S. M. J., Bernardini, E., and Kareem, A. A first step towards a general methodology for the performance-based design of wind-excited structures. *Structures Congress 2015*, 1482-1493, (2015).

[5] Chuang, W. C., and Spence, S. M. J. A performance-based design framework for the integrated collapse and non-collapse assessment of wind-excited buildings. *Engineering Structures*, **150**, 746–758, (2017).

[6] Mohammadi, A., Azizinamini, A., Griffis, L., and Irwin, P. Performance assessment of an existing 47-story high-rise building under extreme wind loads. *Journal of Structural Engineering*, **145**(1), 04018232, (2019).

[7] Chuang, W. C., and Spence, S. M. J. A framework for the efficient reliability assessment of inelastic wind excited structures at dynamic shakedown. *Journal of Wind Engineering and Industrial Aerodynamics*, **220**, 104834, (2021).

[8] Williams, T., and Kareem, A. Performance of building cladding in urban environments under extreme winds. In *Proc., 11th Int. Conf. on Wind Engineering*, (2003).

[9] Kareem, A., and Bashor, R. Performance of glass/cladding of high-rise buildings in Hurricane Katrina. *The Wind Engineer (Newsletter of AAWE)*, 1–5, (2006).

[10] Bedon, C., Zhang, X., Santos, F., Honfi, D., Kozłowski, M., Arrigoni, M., Figuli, L., and Lange, D. Performance of structural glass facades under extreme loads–design methods, existing research, current issues and trends. *Construction and Building Materials*, **163**, 921–937, (2018).

[11] Ouyang, Z., and Spence, S. M. J. A performance-based damage estimation framework for the building envelope of wind-excited engineered structures. *Journal of Wind Engineering and Industrial Aerodynamics*, **186**, 139–154, (2019).

[12] Ouyang, Z., and Spence, S. M. J. A performance-based wind engineering framework for envelope systems of engineered buildings subject to directional wind and rain hazards. *Journal of Structural Engineering*, **146**(5), 04020049, (2020).

[13] Ouyang, Z., and Spence, S. M. J. A performance-based wind engineering framework for engineered building systems subject to hurricanes. *Frontiers in Built Environment*, **7**, 720764, (2021).

[14] Ouyang, Z., and Spence, S. M. J. Performance-based wind-induced structural and envelope damage assessment of engineered buildings through nonlinear dynamic analysis. *Journal of Wind Engineering and Industrial Aerodynamics*, **208**, 104452, (2021).

[15] Arunachalam, S., and Spence, S. M. J. An efficient stratified sampling scheme for the simultaneous estimation of small failure probabilities in wind engineering applications. *Structural Safety*, **101**, 102310, (2023).

[16] American Society of Civil Engineers. Minimum design loads and associated criteria for buildings and other structures. *American Society of Civil Engineers*, (2022).

[17] Mazzoni, S. OpenSees command language manual, (2006).

[18] Xu, L., and Spence, S. M. J. Collapse reliability of wind-excited reinforced concrete structures by stratified sampling and nonlinear dynamic analysis. *Reliability Engineering & System Safety*, **250**, 110244, (2024).

[19] FEMA. Seismic performance assessment of buildings, volume 1, methodology. *FEMA P-58-1*, Washington DC, (2012).

[20] Behr, R. A., Karson, M. J., and Minor, J. E. Reliability analysis of window glass failure pressure data. *Structural Safety*, **11**(1), 43–58, (1991).